Experimental demonstration of enhanced violations of Leggett-Garg inequalities in a $\mathcal{PT}$-symmetric trapped-ion qubit

Pengfei Lu,[1,*] Xinxin Rao,[1,*] Teng Liu,[1] Yang Liu,[1,2] Ji Bian,[1] Feng Zhu,[1,2] and Le Luo[1,2,3,4,†]

[1]*School of Physics and Astronomy, Sun Yat-Sen University, Zhuhai 519082, China*

[2]*Shenzhen Research Institute of Sun Yat-Sen University, Nanshan Shenzhen 518087, China*

[3]*Quantum Science Center of Guangdong-HongKong-Macao Greater Bay Area, Shenzhen 518048, China*

[4]*State Key Laboratory of Optoelectronic Materials and Technologies, Sun Yat-Sen University, Guangzhou 510275, China*

(Received 15 September 2023; revised 16 January 2024; accepted 5 March 2024; published 8 April 2024)

The Leggett-Garg inequality (LGI) delineates a boundary between quantum and classical systems. While the temporal quantum correlations represented by LGIs have been extensively investigated in the Hermitian domain, the exploration of LGIs under non-Hermitian conditions remains scarce. Theoretical conjectures posit that nonunitary dynamics could transcend the boundary of LGIs set by Hermitian quantum mechanics, yet its empirical validation is lacking. Here, we demonstrate the enhanced violation of LGIs in a non-Hermitian system of a parity-time ($\mathcal{PT}$)-symmetric trapped-ion qubit. The upper bounds of both the third-order parameter K_3 and fourth-order parameter K_4 increase with dissipation and can reach the maximum value when the system approaches the exceptional point, where $K_3 = C_{21} + C_{32} - C_{31}$ is comprising three two-time correlations and $K_4 = C_{21} + C_{32} + C_{43} - C_{41}$ is comprising four correlations. We also find that the lower bounds of K_3 and K_4 exhibit distinctive behaviors, where the lower bound of K_3 remains constant, but that of K_4 depends on the target states and measurement operators. These findings reveal a pronounced correlation between the dissipative nature of a quantum system and its temporal correlations.

DOI: 10.1103/PhysRevA.109.042205

I. INTRODUCTION

Quantum state superposition [1] stands as a fundamental concept in quantum mechanics, providing a framework to describe the behavior of particles on microscopic scales. However, the concept of superposition runs counter to the tenets of macrorealism, as exemplified by the renowned "Schrödinger's cat" paradox proposed in 1935 [2]. In a quest to delve into the experimental implications of this paradox, Leggett and Garg introduced the Leggett-Garg inequality (LGI) in 1985 [3]. This inequality aims to delineate the temporal correlation in a classical world, with its validity anchored in two fundamental assumptions: (i) macroscopic realism (MR), asserting that a macroscopic system possesses a definite state at any given time; (ii) noninvasive measurement (NIM), stipulating that measurements should not alter the state of the system. The violation of this inequality in quantum mechanics arises from two primary reasons: first, the principle of quantum superposition contravenes the concept of realism; second, the collapse of quantum states challenges the NIM assumption.

The LGI serves as a tool for testing correlations within a single system at different moments. This is in contrast to the Bell inequality, which is employed to test correlations between spatially separated systems [4]. The most frequently encountered LGI follows a general form [5]

$$K_n = C_{21} + C_{32} + C_{43} + \cdots + C_{n(n-1)} - C_{n1}, \qquad (1)$$

where $C_{n(n-1)}$ represents the correlation function of the observables between times t_n and t_{n-1}. The basic form of third-order LGIs emerges from the measurement of a system with two possible states at three consecutive moments, expressed as $-3 \leqslant K_3 \leqslant 1$. The upper bound of one, often referred to as the classical bound, is constrained by the behavior of classical systems. But in a two-level quantum system, the upper limit of third-order LGI K_3 can reach 1.5, as dictated by the Lüders state update rule (LSUR)—commonly known as the Lüders bound [6]. This boundary is also recognized as the temporal Tsirelson bound (TTB) [7], drawing parallels to Tsirelson's bound in the context of Bell's inequality. For quantum systems with multiple levels, instead of the LSUR, the von Neumann state update rule (VSUR) is commonly employed to project the system to its each subspace. This allows the extraction of information from higher dimensions. Utilizing the VSUR, the upper bound of K_3 can surpass the limitation of 1.5 [8]. Experimental investigations of K_3 have been implemented on closed quantum systems, including superconducting circuits [9], single-photon [10,11], nuclear magnetic resonance [12,13], trapped ions [14], and *NV* centers [15,16].

Higher-order LGIs typically refer to the inequalities that involve two-time correlations of more than three different moments. The higher-order LGIs could discern more differentiation between classical and quantum systems than K_3. For example, the higher-order LGIs are valuable in addressing the clumsiness loophole [17] and they can be related to the cut polytope for a nontrivial test of macrorealism [18]. The elementary higher-order LGI K_4 has been studied theoretically

*These authors contributed equally to this work.

†luole5@mail.sysu.edu.cn

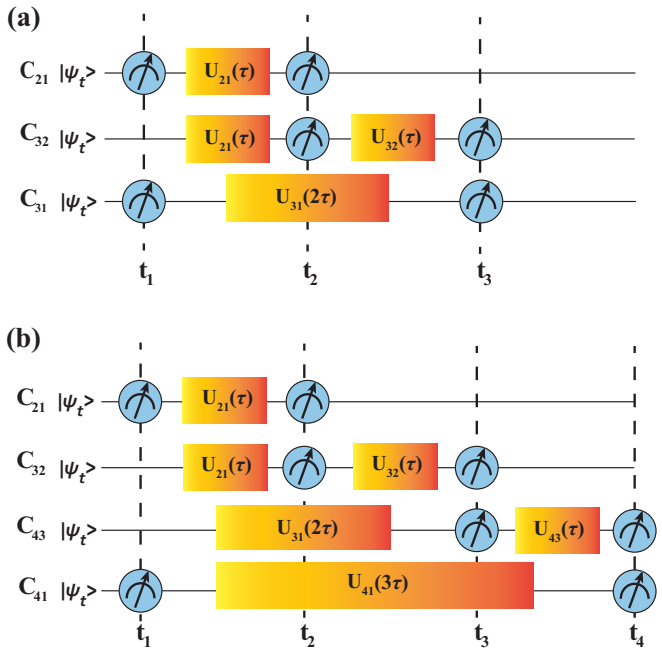

FIG. 1. Schemes of testing third-order (K_3) and fourth-order (K_4) LGIs. (a) The experiment involves measuring three two-time temporal correlations (C_{21}, C_{32}, and C_{31}) to determine the parameter K_3. (b) The experiment requires measuring four two-time temporal correlations (C_{21}, C_{32}, C_{43}, and C_{41}) to determine the parameter K_4. Here, $|\psi_t\rangle$ denotes the target state, the time intervals are defined as $t_j - t_i = (j-i)\tau$, and $t_1 = 0$. The preparation of $|\psi_t\rangle$ can be regarded as the measurement at time t_1.

[19,20]. Its standard expression is articulated as $-2 \leqslant K_4 \leqslant 2$ ($-2\sqrt{2} \leqslant K_4 \leqslant 2\sqrt{2}$) in classical (quantum) systems. Due to both structural and boundary resemblances, K_4 can be viewed as a temporal analog to the Clauser-Horne-Shimony-Holt (CHSH) inequality. The experimental investigation of K_4 in a three-level system has exceeded the constraints set by the TTB [21]. Recently, Halliwell *et al.* [22–24] utilized multitime correlations to explore the criteria for macroscopic realism within fourth-order LGIs.

While the LGIs have been extensively studied in closed quantum systems, their roles in open quantum systems still remain elusive, where the interplay between the quantum dynamics and the coupling to external environment could enhance temporal correlations. This prompts the following intriguing question: can the larger violation (beyond the TTB) of LGIs emerge in an open quantum system? Theoretical studies have predicted that a two-level non-Hermitian system undergoing nonunitary dynamics will lead to enhanced violations of LGIs [25–27], showing that the upper bound of K_3 can approach the algebraic maximum value of 3. The larger violations of LGIs in non-Hermitian systems is the indicator of the enhancement of temporal correlation in an open quantum system. Thanks to the atomic systems with controllable dissipation [28–33], recent experimental investigations of LGIs have been conducted in a non-Hermitian trapped-ion qubit [34,35], utilizing K_3 to quantify enhanced quantum correlation.

Exploring LGIs in non-Hermitian systems is significant for unraveling the intricate interplay between quantum coherence, dissipation, and emergent phenomena [36]. This exploration has implications for both fundamental quantum theory and practical applications in emerging quantum technologies. For fundamental quantum theory, examining LGIs in non-Hermitian systems helps to understand how dissipation and decoherence influence the violation of the realism, providing valuable information about the robustness of quantum features in the presence of environmental interactions [37]. On the other hand, for quantum information processing, a deeper comprehension of the behavior of LGIs in non-Hermitian systems may open up a pathway for the stability of quantum coherence and correlations in the presence of dissipation [25], which is crucial for the development of robust quantum technologies. Particularly, studying LGIs in non-Hermitian systems provides insights into how non-Hermitian dynamics affect the transition from quantum to classical behavior [38], shedding light on the quantum-to-classical crossover of a larger scale system with entanglements and correlations.

In this paper, we systematically investigate the third- and fourth-order LGIs (K_3 and K_4) in a trapped-ion system governed by a parity-time ($\mathcal{PT}$)-symmetric Hamiltonian. The upper bounds for both K_3 and K_4 exhibit the enhanced violations with increasing dissipation. Contrastingly, the lower bounds for K_3 and K_4 manifest distinct behaviors. While K_3 remains constant with increasing dissipation, demonstrating insensitivity to non-Hermiticity, K_4 exhibits variation in response to escalating dissipation. We also find that the lower bound of K_4 depends on both the measurement operator and the target state, which could vary differently with the dissipation. These findings provide a route to finely tune the strength of quantum correlation through nonunitary dynamics.

II. THEORY OF LGIS OF A $\mathcal{PT}$-SYMMETRIC HAMILTONIAN

A. $\mathcal{PT}$-symmetric dynamics of a non-Hermitian qubit

The non-Hermitian LGI test is conducted in a single trapped-ion qubit with a $\mathcal{PT}$-symmetric Hamiltonian ($\hbar = 1$)

$$H_{\mathcal{PT}} = \begin{pmatrix} i\gamma & J \\ J & -i\gamma \end{pmatrix}, \tag{2}$$

where J is the coupling strength and γ is the dissipation rate. The term $i\gamma$ ($-i\gamma$) in the diagonal represents the gain (loss) of the qubit. Equation (2) commutes with the $\mathcal{PT}$ operator [39], i.e., $[H_{\mathcal{PT}}, \mathcal{PT}] = 0$, where $\mathcal{P} = \sigma_x$ and $\mathcal{T} = *$ denotes complex conjugation operation. The eigenvalues can be obtained as $\lambda = \pm J\sqrt{1-S^2}$, where the parameter $S = \gamma/J$ represents the degree of non-Hermiticity. When $0 \leqslant S < 1$, the system is in the $\mathcal{PT}$ symmetry unbroken phase. When $S > 1$, the system is in the $\mathcal{PT}$ symmetry broken phase. The exceptional point locates at $S = 1$. The investigation of $\mathcal{PT}$ symmetry breaking transition can be found in the previous works conducted by our group [33,40] and others [32,41].

The non-Hermitian systems with pure loss provide a convenient way to explore the $\mathcal{PT}$-symmetric dynamic features in quantum systems, given that quantum systems rarely possess the gain terms. The effective $\mathcal{PT}$ Hamiltonian of pure loss

follows as

$$H_{\text{eff}} = H_{\mathcal{PT}} - i\gamma \boldsymbol{I} = \begin{pmatrix} 0 & J \\ J & -2i\gamma \end{pmatrix}, \tag{3}$$

where $\boldsymbol{I}$ is the identity operator. Based on the relation $e^{2\gamma t}|\langle\psi_{\text{fin}}|e^{-iH_{\text{eff}}t}|\psi_{\text{ini}}\rangle|^2 = |\langle\psi_{\text{fin}}|e^{-iH_{\mathcal{PT}}t}|\psi_{\text{ini}}\rangle|^2$, the evolution of non-Hermitian systems, governed by H_{eff}, when multiplied by a coefficient $e^{2\gamma t}$, can be effectively mapped to those of $\mathcal{PT}$-symmetric systems governed by $H_{\mathcal{PT}}$.

B. Third- and fourth-order LGIs in a non-Hermitian system

The schemes of testing the third-order (K_3) and fourth-order (K_4) LGIs under H_{eff} are depicted in Figs. 1(a) and 1(b). The correlation function C_{ji} is derived from the joint probability $P_{ji}(Q_j, Q_i)$ of obtaining the outcome of observable Q_i (Q_j) at time t_i (t_j). The corresponding expression is denoted as

$$C_{ji} = \sum_{q_i, q_j = \pm 1} q_i q_j P_{ji}(Q_j, Q_i), \tag{4}$$

where the macroscopic dichotomic variables $q_i = \pm 1$ (at time t_i) and $q_j = \pm 1$ (at time t_j). Then, we utilize σ_y as the observable for calculating the two-time correlation, with the eigenvectors $|+\rangle = [i/\sqrt{2}, 1/\sqrt{2}]^T$ and $|-\rangle = [-i/\sqrt{2}, 1/\sqrt{2}]^T$ representing the two eigenstates of σ_y. $q_{i,j} = \pm 1$ with $|\pm\rangle$. The joint probability under the $H_{\mathcal{PT}}$ is equivalent to that under H_{eff} as

$$\begin{aligned} P_{ji}(Q_j, Q_i) &= \frac{|\langle Q_j|e^{-iH_{\mathcal{PT}}t_{ji}}|Q_i\rangle|^2}{\langle Q_i|e^{iH_{\mathcal{PT}}^{\dagger}t_{ji}}e^{-iH_{\mathcal{PT}}t_{ji}}|Q_i\rangle} \frac{|\langle Q_i|e^{-iH_{\mathcal{PT}}t_{i1}}|\psi_t\rangle|^2}{\langle\psi_t|e^{iH_{\mathcal{PT}}^{\dagger}t_{i1}}e^{-iH_{\mathcal{PT}}t_{i1}}|\psi_t\rangle} \\ &= \frac{|\langle Q_j|e^{-iH_{\text{eff}}t_{ji}}|Q_i\rangle|^2}{\langle Q_i|e^{iH_{\text{eff}}^{\dagger}t_{ji}}e^{-iH_{\text{eff}}t_{ji}}|Q_i\rangle} \frac{|\langle Q_i|e^{-iH_{\text{eff}}t_{i1}}|\psi_t\rangle|^2}{\langle\psi_t|e^{iH_{\text{eff}}^{\dagger}t_{i1}}e^{-iH_{\text{eff}}t_{i1}}|\psi_t\rangle}, \end{aligned} \tag{5}$$

where $Q_{i,j} = \{+, -\}$ at time $t_{i,j}$, $t_{ji} = t_j - t_i = (j - i)\tau$. This allows for straightforward calculation of $P_{ji}(+,+)$, $P_{ji}(-,+)$, $P_{ji}(+,-)$, and $P_{ji}(-,-)$.

In general, K_3 and K_4 are dependent on the target state $|\psi_t\rangle$. To obtain the maximum violation, we choose $|\psi_t\rangle = |+\rangle$ based on the maximum values of K_3 and K_4 in the θ-ϕ plane (see Appendix A for details). Consequently, K_3 and K_4 in the Hermitian case (in the absence of the dissipation rate γ) are expressed by

$$\begin{aligned} K_3 &= 2\cos(2J\tau) - \cos(4J\tau), \\ K_4 &= 3\cos(2J\tau) - \cos(6J\tau), \end{aligned} \tag{6}$$

while in the non-Hermitian case (with the presence of the dissipation rate γ), the LGIs can be replaced by

$$K_3 = \frac{\gamma + JA}{J + \gamma A} - \frac{\gamma + JB}{J + \gamma B} + \frac{J\gamma^2 + J(J^2 + J\gamma - \gamma^2)A}{(J - \gamma A)(J + \gamma A)^2} - \frac{\gamma A^2(-J^2 + J\gamma + \gamma^2 + J^2 A)}{(J - \gamma A)(J + \gamma A)^2} \tag{7}$$

and

$$\begin{aligned} K_4 = {} & \frac{\gamma + JA}{J + \gamma A} - \frac{\gamma + JC}{J + \gamma C} + \frac{(\gamma + J)(A + 1)(\gamma + JA)}{2(J + \gamma A)^2} - \frac{(J - \gamma)(1 - A)(JA - \gamma)}{\gamma^2 - 2J^2 + \gamma^2 B} \\ & + \frac{2(-\gamma^3 + 2J^3 + \gamma J^2 - 2\gamma^2 J)A + \gamma[2J(J - \gamma)B - J(-2\gamma + JD + J) + 2\chi^2 C]}{4(J - \gamma A)(J + \gamma A)(J + \gamma B)}, \end{aligned} \tag{8}$$

where $\chi = \sqrt{J^2 - \gamma^2}$, $A = \cos(2\tau\chi)$, $B = \cos(4\tau\chi)$, $C = \cos(6\tau\chi)$, and $D = \cos(8\tau\chi)$. The detailed derivations of Eq. (7) and Eq. (8) are provided in Appendix B. Theoretical plots of K_3 and K_4 as a function of γ and τ are also included in Appendix B. The algebraic bounds of K_3 and K_4 in classical, Hermitian, and non-Hermitian conditions can be summarized in Table I.

TABLE I. Algebraic bounds of LGI parameters K_3 and K_4 in classical, Hermitian, and non-Hermitian systems. It is noted that, for the non-Hermitian case, the maximum and minimum values of K_4 can be obtained simultaneously with the certain observable and target state.

Conditions	$K_3^{\min}$	$K_3^{\max}$	$K_4^{\min}$	$K_4^{\max}$
Classical system	-3	1	-2	2
Hermitian system	-3	1.5	$-2\sqrt{2}$	$2\sqrt{2}$
Non-Hermitian system	-3	3[a]	-4[a]	4[a]

[a]The value can be achieved when $\gamma \to J$.

III. EXPERIMENTS AND MEASUREMENTS

A. Trap-ion setup

The LGI experiments were performed employing a single $^{171}Yb^+$ ion. The ion is confined near the center of the trap, which consists of four gold-plated ceramic blade electrodes. The configuration of the microwave and dissipation beam setup is illustrated in Fig. 2(a). To implement Eq. (3), a microwave operating at a frequency of 12.643 GHz and a 369.5 nm dissipative beam are simultaneously applied to the ion. The microwave signal is used to coherently couple the spin states $|0\rangle = |F = 0, m_F = 0\rangle$ and $|1\rangle = |F = 1, m_F = 0\rangle$. The dissipative laser contains only the π polarization component [the purple arrow in Fig. 2(a)] and is used to excite the ion from $|1\rangle$ to the $^2P_{1/2}$ excited state. This excitation leads to spontaneous decay (the blue dashed line) to three magnetic levels $|F = 1, m_F = 0, \pm 1\rangle$ in the $^2S_{1/2}$ ground state with equal probability. The decay to $|F = 1, m_F = \pm 1\rangle$ can be considered as equivalent loss of the qubit, resulting in a nonunitary evolution of the two-level subspace ($|0\rangle$ and $|1\rangle$) [32,33]. The experimental timing sequences are depicted in

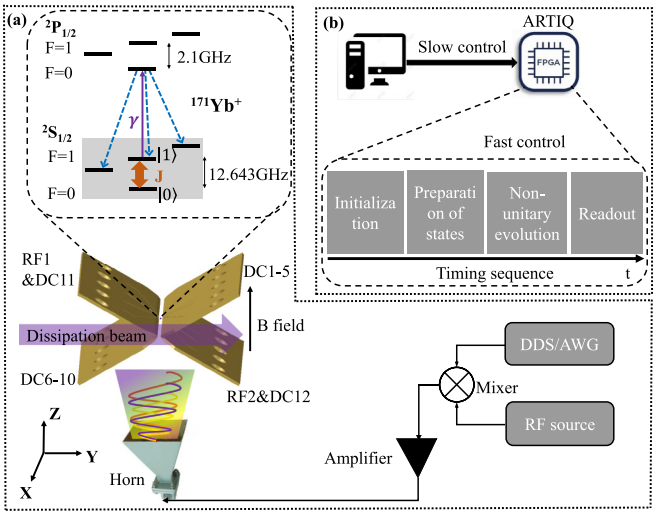

FIG. 2. Experiment setup for testing LGIs. (a) The trap confines a single $^{171}Yb^+$ ion through the application of radio frequency (rf) signals and direct current (dc) voltages to two rf electrodes (RF1 and RF2) and two sets of dc electrodes (DC1-5 and DC6-10), respectively. Additional dc voltages (DC11 and DC12) applied to the rf electrodes are utilized to displace the ion to the rf null position. The magnetic field (**B**) is oriented along the **Z** axis. The microwave signal used to drive the transition between the states $|0\rangle$ and $|1\rangle$ is generated through mixing a standard rf source with either a direct digital synthesizer (DDS) or an arbitrary waveform generator (AWG). The energy level diagram of the $^{171}Yb^+$ ion is depicted within the dashed box; the involved four levels in the gray shaded region can be simplified to a dissipative two-level system. (b) The timing sequences for initialization (including cooling and optical pumping), dissipation beam, and detection beam are controlled by acoustic-optic modulators (AOMs) equipped with rf switches, which receive TTL (transistor transistor logic) sequences from the ARTIQ (advanced real-time infrastructure for quantum physics) device. The synchronization of the microwave and the dissipation laser is precisely controlled by simultaneously triggering and passing through the same length of rf cables. The intensity of the dissipation beam can be finely adjusted by varying the rf power applied on the AOM.

Fig. 2(b). Initially, the ion can be initialized to either $|0\rangle$ or $|1\rangle$ in $^2S_{1/2}$ in the ground-state hyperfine manifold. Next, we prepare the target state and allow for nonunitary evolution for a certain time. Finally, we employ the standard fluorescence counting rate threshold method to readout experimental results.

B. Realization of an effective $\mathcal{PT}$ Hamiltonian

The nonunitary evolution of the multilevel system [the gray shaded region in the inset of Fig. 2(a)] can be described by ($\hbar = 1$)

$$\frac{d\rho}{dt} = -i[H_C, \rho] + \left(L_1\rho L_1{}^\dagger - \frac{1}{2}\{L_1{}^\dagger L_1, \rho\}\right), \qquad (9)$$

where $\rho(t)$ represents a 3×3 density matrix that includes the qubit subspace and $H_C = J(|1\rangle\langle 0| + |0\rangle\langle 1|)$ is a coupling Hamiltonian. $L_1 = \sqrt{4\gamma}|a\rangle\langle 1|$ is the dissipation operator which accounts for the population probability decay from level $|1\rangle$ to $|a\rangle$ ($|a\rangle =^2 S_{1/2}|F=1, m_F=\pm 1\rangle$), where 4γ is the effective dissipation rate from $|1\rangle$ to $|a\rangle$.

Rearranging Eq. (9), we obtain the $d\rho/dt = -i(H_{\rm eff}\rho - \rho H_{\rm eff}^\dagger) + L_1\rho L_1^\dagger$, where the $H_{\rm eff} = H_C - \frac{i}{2}L_1^\dagger L_1$. Because the microwave drive and the dissipation laser beam only act on the qubit, the dynamics of $|a\rangle$ is decoupled from qubit states; therefore, we focus on the qubit subspace of the whole system, where the qubit retains its coherence and its dynamics are governed by the effective $\mathcal{PT}$-symmetric Hamiltonian, and so we neglect the quantum jump term $L_1\rho L_1^\dagger$ and obtain the following:

$$\frac{d\rho}{dt} = \begin{pmatrix} iJ(\rho_{01}-\rho_{10}) & iJ(\rho_{00}-\rho_{11}) - 2\gamma\rho_{01} \\ -iJ(\rho_{00}-\rho_{11}) - 2\gamma\rho_{10} & -iJ(\rho_{01}-\rho_{10}) - 4\gamma\rho_{11} \end{pmatrix}. \qquad (10)$$

In this context, Eq. (10) describes the dynamical evolution of the qubit under the effective Hamiltonian $H_{\rm eff}$ in Eq. (3).

In the experiment, for larger dissipation, the qubit population experiences rapid decay due to spin-dependent loss. This leads to a significantly reduced state population, posing challenges for accurate detection. To address this challenge, we employ a piecewise strategy, where the total evolution time T is partitioned into N segments. In the nth ($1 \leqslant n \leqslant N$) segment, the qubit is prepared to the state predicted by theory, allowing it to evolve for $t_{n-1} = (n-1)T/N$. Subsequently, it continues to evolve for $t = T/N$ under $H_{\rm eff}$. This scheme effectively facilitates the mapping of the entire process.

IV. RESULTS AND DISCUSSION

We observe an enhanced violation in the upper bound of K_3, with its value increasing as the dissipation grows. Figure 3 presents the experimental results of the LGI parameter K_3 under both Hermitian and $\mathcal{PT}$-symmetric dynamics. Figure 3(a) shows the Hermitian case ($\gamma/J = 0$), where $-2.93\,(\pm 0.01) \leqslant K_3 \leqslant 1.51\,(\pm 0.08)$ is obtained from the three correlation functions (see Appendix B). This result aligns with the theoretical calculation represented by the red solid line ($-3 \leqslant K_3 \leqslant 1.5$). The K_3 curves under different dissipation intensities are depicted in Figs. 3(b)–3(d). For $\gamma/J = 0.472$ [Fig. 3(b)], the upper bound of K_3 is $1.79\,(\pm 0.08)$ observed at an evolution time $\tau = 12.5$ μs. The corresponding theoretical value stands at 1.84. Similarly, for $\gamma/J = 0.669$ [Fig. 3(c)], the upper bound of K_3 is 1.91 (± 0.08) observed at $\tau = 14.5$ μs. The corresponding theoretical value stands at 2.10. Increasing dissipation to a higher level, for $\gamma/J = 0.942$ [Fig. 3(d)], the upper bound of K_3 is 2.50 (± 0.11) observed at $\tau = 36.5$ μs, where the corresponding theoretical K_3 value stands at 2.78 approaching the maximum value of 3. It is noted that, as the dissipation increases from the Hermitian case to the exceptional point, the evolution time for the maximum violation increases from $\tau/T_{\rm Rabi} = 1/6$ to $1/4$, where $T_{\rm Rabi} = \pi/\sqrt{J^2-\gamma^2}$ represents the generalized Rabi period with the dissipation. For $\gamma/J = 0.942$, $T_{\rm Rabi} = 144$ μs, and the measured $\tau/T_{\rm Rabi} \simeq 0.25$ is consistent with the prediction. While the upper bound of K_3 surpasses the constraints allowed in the Hermitian system, the lower bound of K_3 remains constant at -3, demonstrating insensitivity to non-Hermiticity.

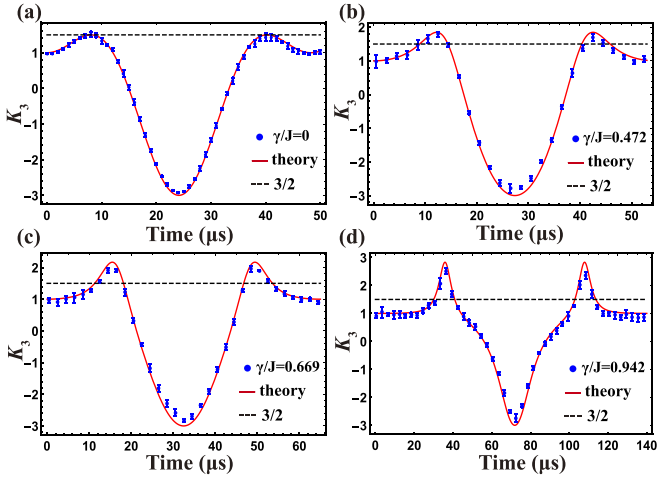

FIG. 3. Experimental results for the LGI parameter K_3. (a) Measurement results of K_3 under Hermitian condition ($\gamma/J = 0$). (b)–(d) Measurement results of K_3 under non-Hermitian condition, with the ratios of γ/J being 0.472 (b), 0.669 (c), and 0.942 (d), respectively. The red solid lines in (a)–(d) are the theoretical results calculated by Eq. (6) [Eq. (7)]. The blue circles depict the experimentally measured results and the dashed line indicates the upper bound (3/2) of K_3 in the quantum system. Error bars for the experimental results are estimated using the standard deviation (1σ) from multiple rounds of experiments. To discern the population information of qubits effectively, each set of experiments is repeated 500 times. The dissipation rates in (a)–(d) correspond to the four dashed lines in Fig. 9(a). The coupling strength J is $2\pi \times 10.4$ kHz.

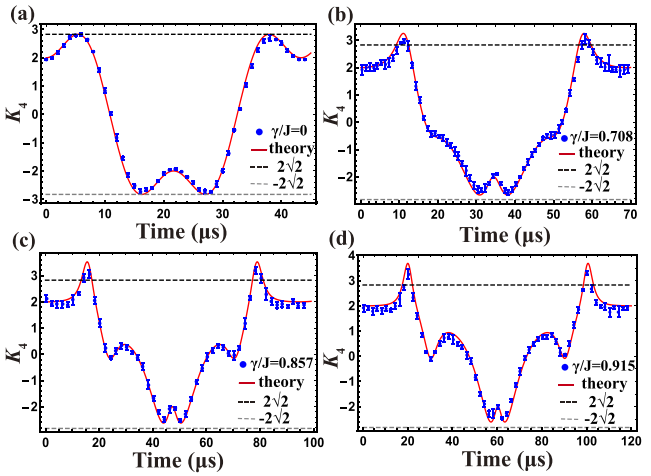

FIG. 4. Experimental results of the LGI parameter K_4. (a) Measurement result of K_4 under Hermitian condition ($\gamma/J = 0$). (b)–(d) Measurement result of K_4 under non-Hermitian condition, with the ratios of γ/J being 0.708 (b), 0.857 (c), and 0.915 (d), respectively. The red solid lines in (a)–(d) are the theoretical results calculated by Eq. (6) [Eq. (8)]. The blue circles depict the experimentally measured results and the black (gray) dashed line is the upper (lower) bound $2\sqrt{2}$ ($-2\sqrt{2}$) of K_4 in the quantum system. The error bars for the experimental results are estimated by the standard deviation (1σ) of multiple rounds of experiments. To discern the population information of qubits effectively, each set of experiments is repeated 500 times. The dissipation rate in (b)–(d) corresponds to three dashed lines in Fig. 9(b). The coupling strengths J in (a) and (b)–(d) are $2\pi \times 11.5$ kHz and $2\pi \times 10.4$ kHz, respectively.

Both the experimental results and the numerical calculations for K_4 are presented in Fig. 4. Figure 4(a) shows the results of the Hermitian dynamics ($\gamma/J = 0$), where $-2.73\,(\pm 0.08) \leqslant K_4 \leqslant 2.82\,(\pm 0.06)$ agrees with the theoretical predictions ($-2\sqrt{2} \leqslant K_4 \leqslant 2\sqrt{2}$) fairly well. Figures 4(b)–4(d) demonstrate enhanced violations of the upper bound for K_4 as the dissipation intensity increases. For $\gamma/J = 0.708$ [Fig. 4(b)], the upper bounds of K_4 observed at $\tau = 11.3$ μs are 2.98 (±0.07). The corresponding theoretical value stands at 3.21. Similarly, for $\gamma/J = 0.857$ [Fig. 4(c)], the upper bound of K_4 is $3.06\,(\pm 0.14)$ at $\tau = 16.3$ μs, compared to the theoretical value of 3.37. In the case of a larger dissipation with $\gamma/J = 0.915$ [Fig. 4(d)], the upper bound of K_4 is 3.25 (±0.20) at $\tau = 20.3$ μs, while the theoretical value is 3.66. For K_4, as the dissipation increases from the Hermitian case to the exceptional point, the evolution time for the maximum violation will increase from $\tau/T_{\text{Rabi}} = 1/8$ to 1/6. For $\gamma/J = 0.915$, $T_{\text{Rabi}} = 120$ μs, and the measured $\tau/T_{\text{Rabi}} \simeq 0.167$.

With the measurement operator σ_y and the target state $|+\rangle$, we observe that the lower bound of K_4 exhibits an upward trend with the increase of dissipation. In the context of a Hermitian system, the lower bound of K_4 is established at $-2\sqrt{2}$ [Fig. 4(a)]. For the case of $\gamma/J = 0.708$ [Fig. 4(b)], the lower bound of K_4 is -2.56 (±0.10) observed at $\tau = 38.3$ μs. The corresponding theoretical value stands at -2.66. Similarly, for $\gamma/J = 0.857$ [Fig. 4(c)], the lower bound of K_4 is -2.52 (±0.06) observed at $\tau = 50.3$ μs. The corresponding theoretical value stands at -2.62. Moving to a larger dissipation level, with $\gamma/J = 0.915$ [Fig. 4(d)], the lower upper bound of K_4 is -2.46 (±0.05) observed at $\tau = 62.3$ μs. The corresponding theoretical value stands at -2.47. The behavior of the lower bound of K_4 is distinguished from that of K_3, which remains constant.

Under the measurement operator σ_y and the target state $|+\rangle$, the lower bound of K_4 does not surpass the Hermitian lower bound. However, the lower bound of K_4 is contingent upon the choice of the observables and target states. In Appendix C, we choose a specific set of the measurement operator and the target state, showing that both the lower and upper bounds of K_4 can be violated simultaneously and reaching the algebraic maximum value of both bounds. These findings indicate that the higher-order LGIs offer specific advantages in certain applications requiring sensitivity to the observables [17,18].

To gain a deeper understanding of the enhanced temporal correlations in non-Hermitian systems, we investigate Eq. (10), which elucidates that the enhanced temporal correlations result from the nonlinear interaction. When we normalize the density matrix ρ, Eq. (10) can be replaced by $d\rho/dt = -iJ[\sigma_x, \rho] + \gamma\{\sigma_z, \rho\} - 2\gamma\langle z\rangle\rho$. The Bloch component $\langle z\rangle = \text{Tr}[\sigma_z\rho]$ characterizes the nonlinear interaction [34,42]. This nonlinear term introduces a nonuniform evolution dynamic, manifested as an inhomogeneous evolution speed illustrated in Fig. 5. This inhomogeneous evolution in the dissipative two-level system has been experimentally confirmed in our previous work [40]. As dissipation increases,

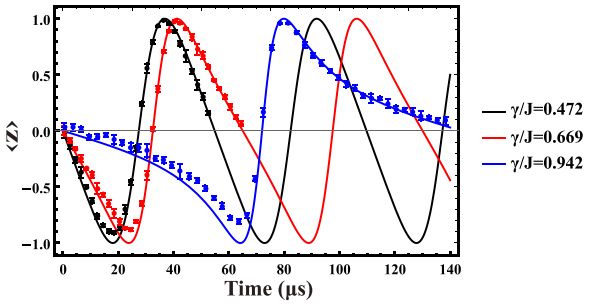

FIG. 5. Experimental results of state evolution dynamic. The three solid lines are theoretical results and different colors represent different dissipation strengths.

the duration of the evolution from $|+\rangle$ to $|1\rangle$ prolongs, while the evolution time from $|1\rangle$ to $|-\rangle$ shortens. This nonuniform speed gives rise to the distorted time-dependent correlations, as evidenced by the evolution from a cosine curve to a non-cosine curve with increasing dissipation (see Appendix B for details). The distorted time-dependent correlations (depicted in Figs. 7 and 8) then result in the larger violations of the LGIs [26].

V. CONCLUSION

We have experimentally demonstrated the enhanced violations of LGIs in a $\mathcal{PT}$-symmetric trapped-ion qubit. The upper bounds of both K_3 and K_4 show enhanced violations with the increasing dissipation, eventually reaching the algebraic maximum values 3 and 4 by infinitely approaching the exceptional point. Intriguingly, we observed that the lower bound of K_3 remains relatively insensitive to non-Hermiticity, while the lower bound of K_4 exhibits remarkable sensitivity to non-Hermiticity, contingent upon the choice of the measurement operators and the target states. Specifically, when

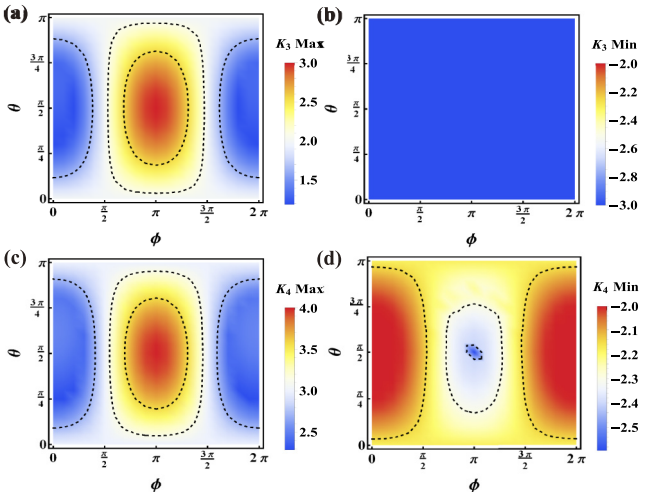

FIG. 6. Numerical results for the maximum and minimum value of K_3 (a),(b) and K_4 (c),(d) by optimizing the parameters θ and ϕ, where the ratio of the coupling strength and dissipation strength approaches the unity ($\gamma/J \to 1$). Here, the observable operator is σ_y.

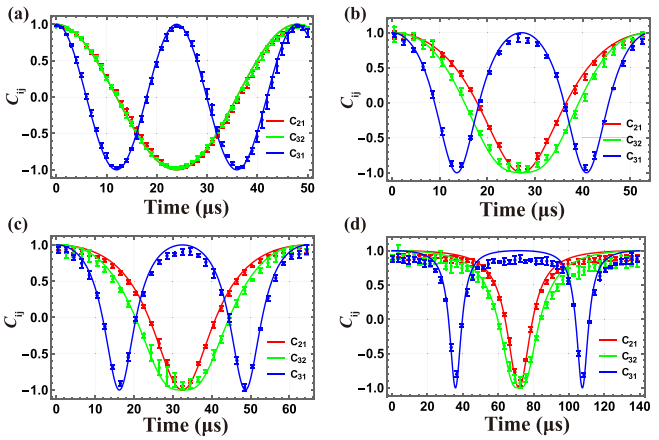

FIG. 7. Experimental results of correlation functions C_{ji} in LG parameter K_3. The dissipation intensity γ in four pictures is (a) 0, (b) $0.472J$, (c) $0.669J$, and (d) $0.942J$, respectively, where the coupling strength J is $2\pi \times 10.4$ kHz.

employing the measurement operator σ_y and the target state $|+\rangle$, the lower bound of K_4 demonstrated an upward trend with increasing dissipation. Furthermore, we conducted experimental investigations of the relation between the nonuniform evolution speed and the enhanced violations of LGIs. Along this line, the LGI tests can be extended to the dissipative quantum many-body systems, holding promise for studying non-Markovian dynamics [43], dissipative quantum phase transitions [44], and quantum-to-classical transition [45].

ACKNOWLEDGMENTS

This work was supported by the National Key Research and Development Program of China (Grant No. 2022YFC2204402), the National Natural Science Foundation of China (Grants No. 11974434 and No. 12074439), the Key-Area Research and Development Program of Guangdong Province (Grant No. 2019B030330001), the

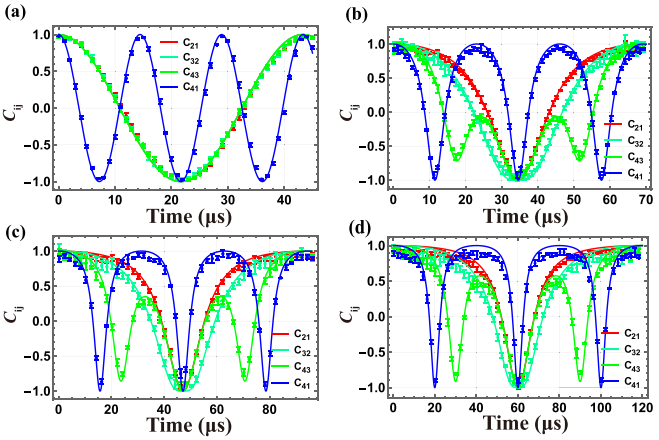

FIG. 8. Experimental results of correlation functions C_{ji} in LG parameter K_4. The dissipation intensity γ in four pictures are (a) 0, (b) $0.708J$, (c) $0.857J$, and (d) $0.915J$, respectively. The coupling strength in (a) is set to $2\pi \times 11.5$ kHz and the coupling strength in (b)–(d) is set to $2\pi \times 10.4$ kHz.

Science and Technology Program of Guangzhou (Grant No. 202102080380), the Shenzhen Science and Technology Program (Grants No. 2021Szvup172 and No. JCYJ20220818102003006), and the Fundamental Research Funds for the Central Universities, Sun Yat-sen University (Grant No. 2021qntd28). L.L. acknowledges the support from Guangdong Province Youth Talent Program (Grant No. 2017GC010656) and Sun Yat-sen University National Defense Research Program. J.B. acknowledges the support from China Postdoctoral Science Foundation (Grant No. 2021M703768). We also thank Qudoor Technology for the support from its trapped-ion quantum computing platform.

APPENDIX A: OPTIMIZATION OF THE TARGET STATE

The selection of the target state is crucial for carrying out an experimental test of LGIs in a dissipative quantum system. In this study, we flip the $|1\rangle$ state to the target state $|\psi_t\rangle$ through the evolution operator

$$U(\theta,\phi)=\begin{pmatrix}\cos\frac{\theta}{2} & -i\,\sin\frac{\theta}{2}e^{-i\phi}\\ -i\,\sin\frac{\theta}{2}e^{i\phi} & \cos\frac{\theta}{2}\end{pmatrix}, \tag{A1}$$

where the $U(\theta,\phi)$ is obtained from the interaction Hamiltonian $H_I=J(\sigma_+e^{i\phi}+\sigma_-e^{-i\phi})(\hbar=1)$ in the rotating frame. Here $\theta=2Jt$ and ϕ are the rotating angle and rotating axis on the Bloch sphere. Thus the target state $|\psi_t\rangle$ can be described as

$$|\psi_t\rangle=U(\theta,\phi)|1\rangle=\begin{pmatrix}-i\,e^{-i\phi}\sin\frac{\theta}{2}\\ \cos\frac{\theta}{2}\end{pmatrix}. \tag{A2}$$

The goal is to obtain the algebraic maximum value of LGIs with the observable σ_y by optimizing the parameters θ and ϕ. To achieve this, we have computed the maximum and minimum values of K_3 and K_4 and presented them in Fig. 6. We find that the optimal solution for the maximum values of K_3 and K_4 is achieved when the parameters are $\theta=\pi/2$ and $\phi=\pi$. The optimal target state is exactly the eigenstate $|+\rangle$ of the observable operator σ_y.

APPENDIX B: CALCULATIONS OF TWO-TIME TEMPORAL CORRELATIONS

The two-time temporal correlations, denoted as C_{ji}, can be calculated through the measurement of the joint probability $P_{ji}(Q_j,Q_i)$. This probability is obtained by preparing the target state $|\psi_t\rangle$ and utilizing the observable operator σ_y. Thus we get the following:

$$\begin{aligned}
C_{21}&=\sum_{q_1,q_2=\pm1}q_1q_2P_{21}(Q_2,Q_1)|_{t_{21}=\tau}=P_{21}(+,+)-P_{21}(-,+)-P_{21}(+,-)+P_{21}(-,-)\\
&=\frac{\gamma+J\,\cos(2\tau\chi)}{J+\gamma\,\cos(2\tau\chi)},\\
C_{31}&=\sum_{q_1,q_3=\pm1}q_1q_3P_{31}(Q_3,Q_1)|_{t_{31}=2\tau}=P_{31}(+,+)-P_{31}(-,+)-P_{31}(+,-)+P_{31}(-,-)\\
&=\frac{\gamma+J\,\cos(4\tau\chi)}{J+\gamma\,\cos(4\tau\chi)},\\
C_{41}&=\sum_{q_1,q_4=\pm1}q_1q_4P_{41}(Q_4,Q_1)|_{t_{41}=3\tau}=P_{41}(+,+)-P_{41}(-,+)-P_{41}(+,-)+P_{41}(-,-)\\
&=\frac{\gamma+J\,\cos(6\tau\chi)}{J+\gamma\,\cos(6\tau\chi)},\\
C_{32}&=\sum_{q_2,q_3=\pm1}q_2q_3P_{32}(Q_3,Q_2)|_{t_{32}=\tau}=P_{32}(+,+)-P_{32}(-,+)-P_{32}(+,-)+P_{32}(-,-)\\
&=\frac{J\gamma^2+J(J^2+J\gamma-\gamma^2)\cos(2\tau\chi)}{[J-\gamma\,\cos(2\tau\chi)][J+\gamma\,\cos(2\tau\chi)]^2}-\frac{\gamma\,\cos^2(2\tau\chi)[-J^2+J\gamma+\gamma^2+J^2\cos(2\tau\chi)]}{[J-\gamma\,\cos(2\tau\chi)][J+\gamma\,\cos(2\tau\chi)]^2},\\
C_{43}&=\sum_{q_3,q_4=\pm1}q_3q_4P_{43}(Q_4,Q_3)|_{t_{43}=\tau}=P_{43}(+,+)-P_{43}(-,+)-P_{43}(+,-)+P_{43}(-,-)\\
&=\frac{2\chi^2(\gamma+2J)\cos(2\tau\chi)}{4[J^2-\gamma^2\cos^2(2\tau\chi)][\gamma\,\cos(4\tau\chi)+J]}+\frac{\gamma[2J(J-\gamma)\cos(4\tau\chi)+2\chi^2\cos(6\tau\chi)]}{4[J^2-\gamma^2\cos^2(2\tau\chi)][\gamma\,\cos(4\tau\chi)+J]}\\
&\quad-\frac{J[-2\gamma+J\,\cos(8\tau\chi)+J]}{4[J^2-\gamma^2\cos^2(2\tau\chi)][\gamma\,\cos(4\tau\chi)+J]}.
\end{aligned} \tag{B1}$$

Here, the time intervals are defined as $t_4-t_3=t_3-t_2=t_2-t_1=\tau$ and $\chi=\sqrt{J^2-\gamma^2}$. The experimentally measured temporal correlations C_{ji} are depicted in Figs. 7 and 8. The experimental results agree well with the corresponding theoretical predictions.

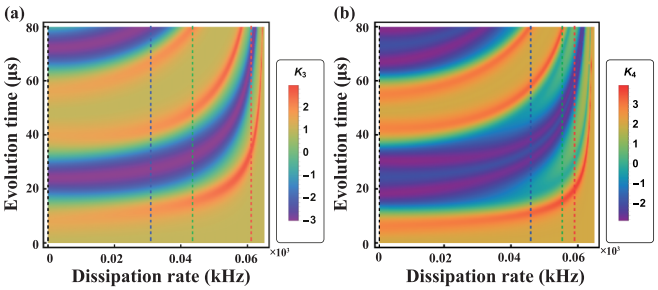

FIG. 9. Theoretical plots of the third-order K_3 (a) and fourth-order K_4 (b) as a function of γ and τ. Here, the target state is $|+\rangle$ and the observable operator is σ_y. The black, blue, green, and red dashed lines in (a) represent $\gamma = 2\pi \times 0$ kHz, $2\pi \times 4.9$ kHz, $2\pi \times 7$ kHz, and $2\pi \times 9.7$ kHz, respectively. Similarly, the black, blue, green, and red dashed lines in (b) represent $\gamma = 2\pi \times 0$ kHz, $2\pi \times 7.3$ kHz, $2\pi \times 8.9$ kHz, and $2\pi \times 9.4$ kHz, respectively. The coupling strength J in (a) and (b) is $2\pi \times 10.4$ kHz.

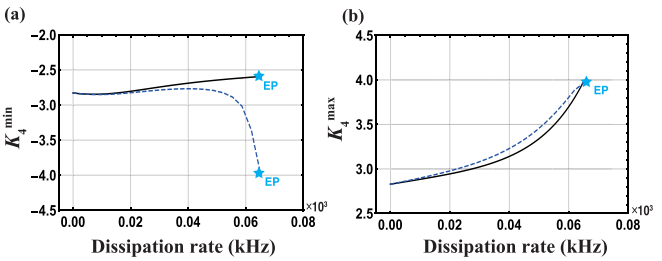

FIG. 10. Numerical results of the higher-order LGI K_4. The lower (a) and upper (b) bounds of K_4 exhibit variations with the dissipation rate under different measurement operators and target states. The parameters for the black solid lines in (a),(b) are $\theta_m = \phi_m = \pi/2$, $\theta = \pi/2$, and $\phi = \pi$. Meanwhile, the parameters for the blue dashed lines in (a),(b) are $\theta_m = \theta = 0.51\pi$, $\phi_m = \pi/2$, and $\phi = \pi$. The coupling strength J in (a) and (b) is $2\pi \times 10.4$ kHz. The exceptional point (EP) is marked by the blue pentagram.

The color maps illustrating the values for K_3 and K_4 as functions of γ and τ are presented in Figs. 9(a) and 9(b). As dissipation increases, the maxima of both K_3 and K_4, represented by red color, shift to larger values. We also observe that the violations of LGIs can approach the algebraic maximum of $K_3^{\max} \to 3$ and $K_4^{\max} \to 4$ when $\gamma \to J$.

APPENDIX C: NUMERICAL RESULTS OF THE HIGHER-ORDER LGI K_4

We analyze variations in the maximum and minimum values of the high-order LGI (K_4) in response to dissipation intensity. This investigation is conducted under various measurement operators and target states, as illustrated in Fig. 10. The universal measurement operator is denoted as

$$\vec{n}\cdot\vec{\sigma} = \begin{pmatrix} \cos(\theta_m) & e^{-i\phi_m}\sin(\theta_m) \\ e^{i\phi_m}\sin(\theta_m) & -\cos(\theta_m) \end{pmatrix}, \tag{C1}$$

where $\vec{n} = [\sin(\theta_m)\cos(\phi_m), \sin(\theta_m)\sin(\phi_m), \cos(\theta_m)]$ is a unit vector in three dimensions and $\vec{\sigma}$ denotes the three component vector of Pauli matrices.

The behavior of the lower bound differs from the case where the lower bound of K_3 remains constant. When $\theta_m = \phi_m = \pi/2$, the measurement operator transforms into σ_y. Following the optimized solution of Eq. (A2), we select $\theta = \pi/2$ and $\phi = \pi$. Under these conditions, we observe an upward trend in the lower (upper) bound of K_4 with increasing dissipation, as depicted by the black solid line in Fig. 10(a) [Fig. 10(b)].

Introducing a new operator ($\theta_m = 0.51\pi$, $\phi_m = \pi/2$) and a new target state using Eq. (A2) ($\theta = 0.51\pi$, $\phi = \pi$) yields distinct results for the lower bound of K_4, as illustrated by the blue dashed line in Fig. 10(a). Meanwhile, the upper bound of K_4 consistently exhibits an upward trend with increasing dissipation [the blue dashed line in Fig. 10(b)]. These findings highlight the strong dependence of the lower bound of K_4 on the selected measurement operator and the target state.

[1] E. Schrödinger, Quantisierung als eigenwertproblem, Ann. Phys. (Leipzig) **385**, 437 (1926).

[2] E. Schrödinger, Die gegenwärtige situation in der quantenmechanik, Naturwissenschaften **23**, 844 (1935).

[3] A. J. Leggett and A. Garg, Quantum mechanics versus macroscopic realism: Is the flux there when nobody looks? Phys. Rev. Lett. **54**, 857 (1985).

[4] J. D. Franson, Bell inequality for position and time, Phys. Rev. Lett. **62**, 2205 (1989).

[5] C. Emary, N. Lambert, and F. Nori, Leggett-Garg inequalities, Rep. Prog. Phys. **77**, 016001 (2014).

[6] G. Lüders, Concerning the state-change due to the measurement process, Ann. Phys. (NY) **518**, 663 (2006).

[7] B. S. Cirel'son, Quantum generalizations of Bell's inequality, Lett. Math. Phys. **4**, 93 (1980).

[8] C. Budroni and C. Emary, Temporal quantum correlations and Leggett-Garg inequalities in multilevel systems, Phys. Rev. Lett. **113**, 050401 (2014).

[9] A. Palacios-Laloy, F. Mallet, F. Nguyen, P. Bertet, D. Vion, D. Esteve, and A. N. Korotkov, Experimental violation of a Bell's inequality in time with weak measurement, Nat. Phys. **6**, 442 (2010).

[10] Z.-Q. Zhou, S. F. Huelga, C.-F. Li, and G.-C. Guo, Experimental detection of quantum coherent evolution through the violation of Leggett-Garg-type inequalities, Phys. Rev. Lett. **115**, 113002 (2015).

[11] J. Dressel, C. J. Broadbent, J. C. Howell, and A. N. Jordan, Experimental violation of two-party Leggett-Garg inequalities with semiweak measurements, Phys. Rev. Lett. **106**, 040402 (2011).

[12] V. Athalye, S. S. Roy, and T. S. Mahesh, Investigation of the Leggett-Garg inequality for precessing nuclear spins, Phys. Rev. Lett. **107**, 130402 (2011).

[13] H. Katiyar, A. Shukla, K. R. Rao, and T. S. Mahesh, Violation of entropic Leggett-Garg inequality in nuclear spins, Phys. Rev. A **87**, 052102 (2013).

[14] T. Zhan, C. Wu, M. Zhang, Q. Qin, X. Yang, H. Hu, W. Su, J. Zhang, T. Chen, Y. Xie *et al.*, Experimental violation of the Leggett-Garg inequality in a three-level trapped-ion system, Phys. Rev. A **107**, 012424 (2023).

[15] G. Waldherr, P. Neumann, S. F. Huelga, F. Jelezko, and J. Wrachtrup, Violation of a temporal Bell inequality for single spins in a diamond defect center, Phys. Rev. Lett. **107**, 090401 (2011).

[16] M. Tusun, W. Cheng, Z. Chai, Y. Wu, Y. Wang, X. Rong, and J. Du, Experimental violation of the Leggett-Garg inequality with a single-spin system, Phys. Rev. A **105**, 042613 (2022).

[17] M. M. Wilde and A. Mizel, Addressing the clumsiness loophole in a Leggett-Garg test of macrorealism, Found. Phys. **42**, 256 (2012).

[18] D. Avis, P. Hayden, and M. M. Wilde, Leggett-Garg inequalities and the geometry of the cut polytope, Phys. Rev. A **82**, 030102(R) (2010).

[19] J. F. Clauser, M. A. Horne, A. Shimony, and R. A. Holt, Proposed experiment to test local hidden-variable theories, Phys. Rev. Lett. **23**, 880 (1969).

[20] T. Fritz, Quantum correlations in the temporal Clauser–Horne–Shimony–Holt (CHSH) scenario, New J. Phys. **12**, 083055 (2010).

[21] K. Wang, C. Emary, X. Zhan, Z. Bian, J. Li, and P. Xue, Enhanced violations of Leggett-Garg inequalities in an experimental three-level system, Opt. Express **25**, 31462 (2017).

[22] J. J. Halliwell, Leggett-Garg tests of macrorealism: Checks for noninvasiveness and generalizations to higher-order correlators, Phys. Rev. A **99**, 022119 (2019).

[23] S. Majidy, J. J. Halliwell, and R. Laflamme, Detecting violations of macrorealism when the original Leggett-Garg inequalities are satisfied, Phys. Rev. A **103**, 062212 (2021).

[24] S.-S. Majidy, H. Katiyar, G. Anikeeva, J. Halliwell, and R. Laflamme, Exploration of an augmented set of Leggett-Garg inequalities using a noninvasive continuous-in-time velocity measurement, Phys. Rev. A **100**, 042325 (2019).

[25] H. S. Karthik, H. A. Shenoy, and A. R. U. Devi, Leggett-Garg inequalities and temporal correlations for a qubit under PT-symmetric dynamics, Phys. Rev. A **103**, 032420 (2021).

[26] A. V. Varma, I. Mohanty, and S. Das, Temporal correlation beyond quantum bounds in non-Hermitian PT-symmetric dynamics of a two level system, J. Phys. A: Math. Theor. **54**, 115301 (2021).

[27] A. V. Varma, J. E. Muldoon, S. Paul, Y. N. Joglekar, and S. Das, Extreme violation of the Leggett-Garg inequality in nonunitary dynamics with complex energies, Phys. Rev. A **108**, 032202 (2023).

[28] J. Li, A. K. Harter, J. Liu, L. de Melo, Y. N. Joglekar, and L. Luo, Observation of parity-time symmetry breaking transitions in a dissipative Floquet system of ultracold atoms, Nat. Commun. **10**, 855 (2019).

[29] J. T. Barreiro, M. Müller, P. Schindler, D. Nigg, T. Monz, M. Chwalla, M. Hennrich, C. F. Roos, P. Zoller, and R. Blatt, An open-system quantum simulator with trapped ions, Nature (London) **470**, 486 (2011).

[30] D. Kienzler, H.-Y. Lo, B. Keitch, L. De Clercq, F. Leupold, F. Lindenfelser, M. Marinelli, V. Negnevitsky, and J. P. Home, Quantum harmonic oscillator state synthesis by reservoir engineering, Science **347**, 53 (2015).

[31] P. M. Harrington, E. J. Mueller, and K. W. Murch, Engineered dissipation for quantum information science, Nat. Rev. Phys. **4**, 660 (2022).

[32] L. Ding, K. Shi, Q. Zhang, D. Shen, X. Zhang, and W. Zhang, Experimental determination of PT-symmetric exceptional points in a single trapped ion, Phys. Rev. Lett. **126**, 083604 (2021).

[33] J. Bian, P. Lu, T. Liu, H. Wu, X. Rao, K. Wang, Q. Lao, Y. Liu, F. Zhu, and L. Luo, Quantum simulation of a general anti-PT symmetric hamiltonian with a trapped ion qubit, Fundam. Res. **3**, 904 (2023).

[34] C.-W. Wu, M.-C. Zhang, Y.-L. Zhou, T. Chen, R. Huang, Y. Xie, B.-Q. Ou, W. Wu, A. Miranowicz, J. Zhang *et al.*, Maximizing temporal quantum correlation by approaching an exceptional point, arXiv:2304.06590.

[35] A. Quinn, J. Metzner, J. E. Muldoon, I. D. Moore, S. Brudney, S. Das, D. T. Allcock, and Y. N. Joglekar, Observing superquantum correlations across the exceptional point in a single, two-level trapped ion, arXiv:2304.12413.

[36] C. Emary, Decoherence and maximal violations of the Leggett-Garg inequality, Phys. Rev. A **87**, 032106 (2013).

[37] M. Łobejko, J. Łuczka, and J. Dajka, Leggett-Garg inequality for qubits coupled to thermal environment, Phys. Rev. A **91**, 042113 (2015).

[38] Y. Zhang and X. Tan, Leggett–Garg inequality, wigner form of Leggett–Garg inequality and no-signaling-in-time condition under coarsening measurement, Quantum Inf. Process. **21**, 157 (2022).

[39] C. M. Bender and S. Boettcher, Real spectra in non-Hermitian Hamiltonians having PT symmetry, Phys. Rev. Lett. **80**, 5243 (1998).

[40] P. Lu, Y. Liu, X. Rao, Q. Lao, H. Wu, F. Zhu, L. Luo *et al.*, Realizing quantum speed limit in open system with a PT-symmetric trapped-ion qubit, New J. Phys. **26**, 013043 (2024).

[41] W.-C. Wang, Y.-L. Zhou, H.-L. Zhang, J. Zhang, M.-C. Zhang, Y. Xie, C.-W. Wu, T. Chen, B.-Q. Ou, W. Wu, H. Jing, and P. X. Chen, Observation of PT-symmetric quantum coherence in a single-ion system, Phys. Rev. A **103**, L020201 (2021).

[42] D. C. Brody and E.-M. Graefe, Mixed-state evolution in the presence of gain and loss, Phys. Rev. Lett. **109**, 230405 (2012).

[43] A. M. Souza, J. Li, D. O. Soares-Pinto, R. S. Sarthour, S. Oliveira, S. F. Huelga, M. Paternostro, and F. L. Semião, Experimental demonstration of non-Markovian dynamics via a temporal Bell-like inequality, arXiv:1308.5761.

[44] F. J. Gómez-Ruiz, J. J. Mendoza-Arenas, F. J. Rodríguez, C. Tejedor, and L. Quiroga, Quantum phase transitions detected by a local probe using time correlations and violations of Leggett-Garg inequalities, Phys. Rev. B **93**, 035441 (2016).

[45] A. Zavatta, S. Viciani, and M. Bellini, Quantum-to-classical transition with single-photon-added coherent states of light, Science **306**, 660 (2004).